

# Revisiting Thomson's model with multiply charged superfluid helium nanodroplets

Ernesto García-Alfonso,<sup>1</sup> Francesco Ancilotto,<sup>2,3</sup> Manuel Barranco,<sup>4,5</sup> Fausto Cargnoni,<sup>6</sup> Nadine Halberstadt,<sup>7</sup> and Martí Pi<sup>4,5</sup>

<sup>1</sup>*Laboratoire Collisions, Agrégats, Réactivité (LCAR), Université de Toulouse, CNRS, 31062 Toulouse, France*

<sup>2</sup>*Dipartimento di Fisica e Astronomia "Galileo Galilei" and CNISM, Università di Padova, via Marzolo 8, 35122 Padova, Italy*

<sup>3</sup>*CNR-Istituto Officina dei Materiali (IOM), via Bonomea, 265 - 34136 Trieste, Italy*

<sup>4</sup>*Departament FQA, Facultat de Física, Universitat de Barcelona, Av. Diagonal 645, 08028 Barcelona, Spain.*

<sup>5</sup>*Institute of Nanoscience and Nanotechnology (IN2UB), Universitat de Barcelona, Barcelona, Spain.*

<sup>6</sup>*CNR-SCITEC, Via Golgi 19, 20133 Milano, Italy.*

<sup>7</sup>*Laboratoire Collisions, Agrégats, Réactivité (LCAR), Université de Toulouse, CNRS, 31062, Toulouse, France*

(Dated: 23 October 2024)

We study superfluid helium droplets multiply charged with  $\text{Na}^+$  or  $\text{Ca}^+$  ions. When stable, the charges are found to reside in equilibrium close to the droplet surface, thus representing a physical realization of Thomson's model. We find the minimum radius of the helium droplet that can host a given number of ions using a model whose physical ingredients are the solvation energy of the cations, calculated within the He-DFT approach, and their mutual Coulomb repulsion energy. Our model goes beyond the often used liquid drop model, where charges are smeared out either within the droplet or on its surface, and which neglects the solid-like helium shell around the ions. We find that below a threshold droplet radius  $R_0$ , the total energy of the system becomes higher than that of the separated system of the pristine helium droplet and the charges embedded in their solvation microcluster ("snowball"). However, the ions are still kept within the droplet by the presence of energy barriers which hinder Coulomb explosion. A further reduction of the droplet radius below a value  $R_{expl}$  eventually results in the disappearance of such barrier, leading to Coulomb explosion. Surprisingly, our results are rather insensitive to the ion atomic species. This makes room to discuss them in the context of intrinsic multicharged helium droplets, where the charges are triatomic  $\text{He}_3^+$  ions. Our calculated values for  $R_{expl}$  display the correct scaling with the number of cations compared to available experimental results, at variance with other estimates for the critical radii.

## I. INTRODUCTION

Multiply charged helium nanodroplets have been expected to undergo a fission-like process due to Coulomb repulsion between charges. Consequently, the possibility of creating multiply charged helium droplets that could be stable or metastable in the millisecond time range spanned in usual experiments<sup>1</sup> had seldom been considered, except for doubly charged helium drops produced by electron impact.<sup>2</sup> In that work, doubly positively charged  $\text{He}_N^{2+}$  drops were found for  $N$  larger than  $N \sim 2 \times 10^5$ . The situation has recently changed. Using a novel experimental setup, Laimer *et al.*<sup>3</sup> and Feinberg *et al.*<sup>4</sup> have shown that superfluid helium drops hosting several tens of positive charges can readily be formed by electron impact, and that these drops are stable on the millisecond timescale of the experiment. The radii  $R$  of these multiply charged droplets were determined as a function of the charge state  $n$ , showing that  $R \propto n^{1/2}$ . Since these studies involved pure drops, the ions generated were intrinsic ions. In a theoretical study using a density functional approach specific to superfluid helium (He-DFT),<sup>5</sup> the linear, covalently-bound  $\text{He}_3^+$  cluster ion was identified as the core of a local arrangement characterized by an important enhancement of helium density, usually called "snowball".  $\text{He}_3^+$  ions produced by electron impact in large droplets,  $N \gtrsim 10^5$ , initially appear in the region of

the drop facing the electron source<sup>3,6</sup> and quickly move due to Coulomb repulsion, until reaching their lowest energy configuration on the droplet surface. The ionization of pure helium nanodroplets has been discussed in Ref. 7; see also Ref. 8. The case of negatively charged helium droplets is completely different as, because of Pauli's principle, bubbles of  $\sim 19$  Å radius void of helium atoms are formed around the negative charge<sup>9-11</sup> and are quickly ejected out of the droplet.

Highly charged helium nanodroplets could also be produced by doping them with neutral atomic impurities and subsequently ionizing them. One interesting possibility is to start from droplets doped with several alkali (Ak) atoms, which are known to reside in dimples on the droplet surface.<sup>12-14</sup> The number of Ak dopants can be adjusted by choosing the appropriate doping conditions.<sup>1</sup> Once equilibrated, they can then be photo-ionized, yielding a full-extrinsic multiply charged helium drop. The heavier Ca, Sr and Ba alkaline earth atoms have also been shown to reside at the droplet surface, in a deeper dimple than that of Ak atoms.<sup>15</sup> They should thus behave as Ak atoms in the production of multiply charged helium droplets. It must be noticed that alkali or alkali-earth atoms tend to form dimers or even larger clusters on the droplet surface.<sup>8,16-18</sup> This can in principle be avoided by using large droplets and appropriate doping conditions (low pressure). As an alternative to the photo-ionization of multiple

dopants, one might consider multiply charging a pure helium droplet before the pickup chamber:<sup>4,19</sup> doping will then preferentially occur at the charged sites on the droplet surface and dopant ionization will proceed by charge transfer from  $\text{He}_3^+$  ions.

Whereas the equilibrium position of one single  $\text{Ak}^+$  ion in a  $\text{He}_N$  droplet is at the center,<sup>20</sup> multiple ions –if they can coexist– are expected to be evenly distributed close to the droplet surface. This follows from the balance between  $\text{Ak}^+$ - $\text{Ak}^+$  Coulomb repulsion and droplet- $\text{Ak}^+$  attraction. Beyond a critical  $n$  value, the  $(\text{Ak}^+)_n\text{He}_N$  drop will no longer be stable and  $\text{Ak}^+\text{He}_M$  microclusters with  $M \ll N$  will be ejected. The same is expected for the heavier alkaline earth cations. Charge location for intrinsic multiply charged droplets has recently been determined by X-ray coherent diffractive imaging with Xe as a contrast agent. Xe atoms clustered around the charges, revealing their distribution on the drop surface.<sup>4</sup> Hence, multiply charged helium droplets constitute a realistic model system for Thomson’s problem, i.e., for determining the minimum Coulomb energy configuration of  $n$  charges constrained to remain on the surface of a sphere.<sup>21,25</sup> So far, only negative charges under the form of multielectron bubbles in superfluid helium<sup>22–24</sup> have been studied in this context. Since electron-helium interaction is repulsive, whereas the interaction of helium with a positive charge is strongly attractive, significant differences can be expected in the surface structure and stability of these multiply charged spherical objects.

The liquid drop model (LDM), successfully used to study nuclear fission,<sup>26</sup> has also been applied to address Coulomb fragmentation of charged Van der Waals<sup>27</sup> and simple metal clusters,<sup>28,29</sup> assuming that the process is triggered by Rayleigh instability:<sup>30</sup> if the charge density reaches a threshold value, the drop breaks up into two daughter charged droplets of similar size due to Coulomb repulsion. To compute the Coulomb contribution to the total energy, the LDM usually assumes that the elementary charges are distributed uniformly within the system. Therefore, its application to the present problem is little justified,<sup>31</sup> since charges are localized and Coulomb explosion proceeds by ejection of charged helium microclusters and not by droplet fission.<sup>3</sup> In addition, these microclusters (Atkins’ snowballs) are highly structured around the charge. We propose here a different model based on the He-DFT approach<sup>32–35</sup> that circumvents the use of the LDM in conjunction with Rayleigh’s stability criterion for charged liquid drops. It also has the additional advantage of realistically describing the snowball structure.

Determining the minimum electrostatic energy configuration of  $n$  equal point charges constrained to the surface of a unit sphere (Thomson’s problem) is a classical problem that has no mathematically exact solutions except for a few cases: antipodal points across a diameter for  $n = 2$ ; an equilateral triangle at the equator for  $n = 3$ ; a regular tetrahedron for  $n = 4$ ; a triangular bipyramid for  $n = 5$ ; a regular octahedron for  $n = 6$ ; and a regular icosahedron for  $n = 12$ . For the general case, global minimization of the electrostatic energy has to be performed numerically. The solutions for different  $n$  values can be found in, e.g., Refs. 21 and 25.

In this work we address the structure and energetics of ex-

trinsic multiply charged helium droplets. We design a model based on solvation energy determination within the He-DFT approach, to which Coulomb energy is added. The model is then applied to  $\text{Na}^+$  and  $\text{Ca}^+$  ions as case studies. Na or Ca atoms are assumed to be initially far enough apart on the droplet surface that no dimer nor larger cluster is formed prior to ionization.

This manuscript is organized as follows. In Sec. II we introduce the solvation plus Coulomb model proposed in this work. The application of the He-DFT approach to a doped planar helium surface (as a model for the surface of a very large droplet) is described in Sec. III. Results are presented and discussed in Sec. IV, and a summary of the results is presented in Sec. VI together with some concluding remarks. Finally, the Appendix describes the determination of the *ab initio*  $\text{Ca}^+$ -He potential used in this work.

## II. THE SOLVATION PLUS COULOMB APPROACH

A full He-TDDFT simulation of a multiply charged droplet is computationally not feasible because of the large size required for droplets to host even a small number  $n$  of charges.<sup>3</sup> To circumvent this limitation, we have designed a model based on a crucial input: the *solvation energy* of the ion, which we calculate using the He-DFT method. This model is described in the following.

The condition for the existence of a stable configuration of  $n$  charges  $\text{A}^+$  in a spherical helium droplet of radius  $R$ ,  $n\text{A}^+@ \text{He}_R$ , is that its formation energy must be negative, i.e., the total energy of the ion-doped helium drop,  $E[n\text{A}^+@ \text{He}_R]$ , must be lower than that of the reference system formed by  $\text{He}_R$  and the  $n$  charges at infinite distance from the droplet and from each other,  $E[\text{He}_R] + nE_{\text{micro}}$

$$E[n\text{A}^+@ \text{He}_R] - E[\text{He}_R] - nE_{\text{micro}} \leq 0 \quad (1)$$

Note that the separated charges of reference can be bare  $\text{A}^+$  or embedded in a microcluster of helium atoms to be defined below, hence their energy is denoted by  $E_{\text{micro}}$ .

Assuming that all the charges are sitting at a distance  $d$  from the droplet surface, defined as the “sharp density” surface (where the helium atom density equals  $\rho_0/2$  with  $\rho_0 = 0.0218 \text{ \AA}^{-3}$  the bulk liquid helium density), the total energy can be expressed as

$$E[n\text{A}^+@ \text{He}_R] = E_d[n\text{A}^+@ \text{He}_R] + E_{\text{Coul}}[n\text{A}^+](R+d), \quad (2)$$

where  $E[n\text{A}^+@ \text{He}_R]$  has been split into the interaction energy of the ions with the helium droplet,  $E_d[n\text{A}^+@ \text{He}_R]$ , and the Coulomb repulsion energy between ions,  $E_{\text{Coul}}[n\text{A}^+](R+d)$ . It is the attractive helium-ion interaction that makes it possible for the multicharged drop to be stable.

Let us define the solvation energy  $S_d[n\text{A}^+@ \text{He}_R]$  of  $n$  positive ions in a helium droplet of radius  $R$  as

$$S_d[n\text{A}^+@ \text{He}_R] = E_d[n\text{A}^+@ \text{He}_R] - E[\text{He}_R] - nE_{\text{micro}} \quad (3)$$

If the droplet is large enough that the interaction energy of one cation with the droplet is not affected by the presence of the

others, the solvation energy of  $nA^+$  simplifies to

$$S_d[nA^+@He_R] \simeq nS_d[A^+@He_R] \quad (4)$$

where the zero for energies is taken as  $E[He_R]$  for convenience. The condition for stability (1) can then be expressed as

$$nS_d[A^+@He_R] + E_{Coul}[nA^+](R+d) \leq 0 \quad (5)$$

For  $n$  cations and a droplet of radius  $R$ , if a distance  $d$  can be found such that inequality (5) is fulfilled, the multicharged droplet will be stable, i.e., will form a bound system. Note that  $d$  can be positive or negative.

It is worth recalling that in order to obtain the stability condition (5), we have implicitly assumed that the droplet is large enough and that all charges are at the same distance from the sharp density surface. In particular, the charge distribution is assumed to be the solution of Thomson's model on a sphere with radius  $R+d$ . We will check in the following that this is a very reasonable approximation.

Calculating  $S_d(A^+@He_R)$  for large  $R$  values can be very time consuming, especially if this has to be done for many different  $R$  values and locations of the ions with respect to the droplet surface. On the other hand, for big enough drops, curvature effects are small and can be safely neglected.  $S_d(A^+@He_R)$  can then be approximated by replacing the drop with a planar helium surface (PHeS). In this case, the grand potential  $\Omega = E - \mu N$  has to be considered rather than the energy, yielding

$$\begin{aligned} S_d(A^+@He_R) &\simeq S_d(A^+@PHeS) \\ &= \Omega_d[A^+@PHeS] - \Omega[PHeS] - \Omega_{micro}(6) \end{aligned}$$

Hence the problem is reduced to determining the grand potential  $\Omega_d[A^+@PHeS]$  for the ion at different distances  $d$  from the sharp density surface of the PHeS, the grand potential of the pristine PHeS, and that of the microcluster structure, all evaluated at the chemical potential of bulk liquid helium at zero temperature and pressure.

The grand potentials are expressed as

$$\begin{aligned} \Omega_d[A^+@PHeS] &= \int d\mathbf{r} [\mathcal{E}_d(A^+@PHeS) - \mu \rho_d(A^+@PHeS)] \\ \Omega[PHeS] &= \int d\mathbf{r} [\mathcal{E}(PHeS) - \mu \rho(PHeS)] \quad (7) \\ \Omega_{micro} &= \int d\mathbf{r} [\mathcal{E}(A^+He_n) - \mu \rho(A^+He_n)], \end{aligned}$$

where  $\mathcal{E}$  is the energy density,  $\mu$  is the chemical potential of bulk liquid helium at zero temperature and pressure (-7.145 K for the functional we are using<sup>36</sup>),  $\rho$  is the helium atom density, and  $d$  is the distance of the ion to the sharp density surface of the PHeS. Finally,  $\Omega_{micro}$  is the grand potential of the microcluster, which is then defined as the cluster of  $M$  heliums around the cation, with  $M$  determined such that the chemical potential is equal to that of bulk liquid helium.

Since we are assuming that the charges are distributed according to the solutions of Thomson's model, the Coulomb

energy can be written as<sup>21</sup>

$$E_{Coul}[nNa^+] = \frac{e^2}{4\pi\epsilon_0} \frac{\xi_n}{R+d}, \quad (8)$$

where  $e$  is the elementary charge and  $\epsilon_0$  the vacuum electric permittivity. The parameter  $\xi_n$  depends on the number of charges  $n$ , for instance:  $\xi_2 = 1/2$ ,  $\xi_3 = \sqrt{3}$ ,  $\xi_4 = 3\sqrt{6}/2$ .  $\xi_n$  values up to  $n = 65$  are tabulated in Ref. 21;  $\xi_n$  values for larger  $n$  can be found in Ref. 25.

The stability of a multicharged droplet is therefore determined by the function

$$U(r) = nS_d[A^+@PHeS] + \frac{e^2}{4\pi\epsilon_0} \frac{\xi_n}{R+d}, \quad (9)$$

where  $r = R+d$  is the distance of the charges to the center of the droplet (recall that  $d$  may be negative or positive).  $U(r)$  is the formation energy –referred to the infinitely separated droplet and ion microclusters– of a droplet of radius  $R$  hosting  $n$  charges at a distance  $d$  from its sharp density surface. A distribution of charges with a common distance  $r$  from the center of the droplet will be energetically stable as long as  $U(r) < 0$ . Therefore, the stability limit for a droplet containing  $n$  charges corresponds to the *smallest* value  $R_0$  of its radius for which  $U(r) = 0$ . This yields

$$R_0(n) = \min_{\{d\}} \left\{ \frac{e^2}{4\pi\epsilon_0} \frac{\xi_n}{n|S_d[A^+@PHeS]|} - d \right\} \quad (10)$$

For  $R > R_0(n)$ , solvation energy will dominate over Coulomb repulsion so that the energy of the system will be negative and the system will be stable. For  $R < R_0$ , electrostatic repulsion will dominate over solvation energy and the energy of the system will be positive: the system is then expected to be unstable against Coulomb explosion. It is thus tempting to interpret  $R_0(n)$  as the critical size observed in experiments.<sup>3,4</sup> As will be seen in the following, the existence of energy barriers preventing Coulomb dissociation of the charged system drastically changes this simple perspective.

An essential ingredient in Eqs. (9-10) is the solvation energy for one single ion at a distance  $d$  from the planar helium surface,  $S_d[A^+@PHeS]$ . It is obtained by carrying out constrained He-DFT calculations similar to those employed for helium drops.<sup>37-39</sup> In the next section we describe in some detail the procedure before discussing the consequences of Eq. (9).

### III. HE-DFT DESCRIPTION OF THE DOPED HELIUM PLANAR SURFACE

Helium density functional theory (He-DFT), in its static and in its time-dependent versions, has proven to be a very powerful tool to study the properties of superfluid <sup>4</sup>He samples. It is a phenomenological approach which constitutes a good compromise between accuracy and feasibility. A detailed description of the method, mainly applied to the study of helium droplets, can be found in Refs. 33–35. Within the

He-DFT approach, the finite range of the helium-helium van der Waals interaction is explicitly incorporated, and surface properties of liquid helium, in particular its surface tension, are well reproduced. We have carried out calculations for  $\text{Na}^+$  and  $\text{Ca}^+$  ions doping a PHeS within He-DFT in order to obtain  $\Omega_d[\text{Na}^+ @ \text{PHeS}]$  and  $\Omega_d[\text{Ca}^+ @ \text{PHeS}]$ , as defined in the previous Section. Here we outline the method we have used for the calculations.

In the static calculations carried out in this work, the ions are described classically, hence their influence on the helium samples is described as an external field.<sup>34</sup> Within the He-DFT approach at zero temperature, the energy of a  $N$ -atom helium sample  ${}^4\text{He}_N$  doped with an  $\text{A}^+$  ion located at  $\mathbf{r}_{\text{A}^+}$  is written as a functional of the  ${}^4\text{He}$  atom density  $\rho(\mathbf{r})$  as

$$E[\Psi, \mathbf{r}_{\text{A}^+}] = \int d\mathbf{r} \frac{\hbar^2}{2m_{\text{He}}} |\nabla\Psi|^2 + \int d\mathbf{r} \mathcal{E}_c(\rho) + \int d\mathbf{r} V_{\text{He-A}^+}(|\mathbf{r} - \mathbf{r}_{\text{A}^+}|) \rho(\mathbf{r}), \quad (11)$$

where the first term is the kinetic energy of the superfluid,  $m_{\text{He}}$  is the mass of the  ${}^4\text{He}$  atom, and  $\Psi(\mathbf{r})$  is the effective wave function (or order parameter) of the superfluid such that  $\rho(\mathbf{r}) = |\Psi(\mathbf{r})|^2$  with  $\int d\mathbf{r} |\Psi(\mathbf{r})|^2 = N$ . The functional  $\mathcal{E}_c(\rho)$  we have used contains the He-He interaction term within the Hartree approximation and additional terms describing non-local correlation effects.<sup>36</sup> It is a modification of the Orsay-Trento functional<sup>32</sup> which makes it stable even in the presence of very attractive impurities. The interaction of one single helium atom with the  $\text{Na}^+$  ion has been taken from Koutselos et al.,<sup>40</sup> while in the case of  $\text{Ca}^+$  it has been calculated *ab initio* and fitted to an analytical form as indicated in the Appendix.

As already stated above, for the PHeS the grand potential  $\Omega = E - \mu N$  has to be minimized rather than the energy, with  $\mu$  the helium chemical potential at zero temperature and pressure (-7.145 K). This guarantees the correct asymptotic density in the bulk of the liquid helium. The equilibrium density in the presence of an  $\text{A}^+$  ion is obtained by solving the Euler-Lagrange (EL) equation resulting from functional variation of the grand potential with  $E$  given by Eq. (11), namely

$$\mathcal{H}[\rho]\Psi = \mu\Psi, \quad (12)$$

where  $\mathcal{H}$  is the DFT Hamiltonian

$$\mathcal{H} = -\frac{\hbar^2}{2m_{\text{He}}} \nabla^2 + \frac{\delta\mathcal{E}_c}{\delta\rho(\mathbf{r})} + V_{\text{He-A}^+}(|\mathbf{r} - \mathbf{r}_{\text{A}^+}|) \quad (13)$$

The effective wave function  $\Psi(\mathbf{r})$  is determined at the nodes of a three-dimension Cartesian grid of 0.3 Å space step inside a large calculation box. The EL equation has been solved by a relaxation (imaginary time  $\tau$ ) method using a modified version of the  ${}^4\text{He}$ -DFT BCN-TLS computing package<sup>41</sup> (see Refs. 34 and 35 and references therein for additional details) adapted to the PHeS geometry. Schematically, the relaxation method proceeds as  $\Psi(\tau + \delta\tau) = \Psi(\tau) + \delta\Psi(\tau)$ , with

$$\delta\Psi(\tau) = -\frac{\delta\tau(\mathcal{H} - \mu)}{1 - (\langle\mathcal{H}\rangle - \mu)\delta\tau} \Psi(\tau), \quad (14)$$

where  $\langle\mathcal{H}\rangle = \langle\Psi(\tau)|\mathcal{H}|\Psi(\tau)\rangle$ . We have imposed specular symmetry at the surface of the box in all three Cartesian coordinates, i.e., continuity of the helium density and cancellation of its first derivative. This allows us to use cosine Fast Fourier Transform<sup>42</sup> to efficiently compute the convolutions needed to obtain the DFT mean field  $\mathcal{H}[\rho]$ . The differential operators in  $\mathcal{H}[\rho]$  are approximated by 13-point formulas.

In order to fix the planar helium surface at an arbitrary location such that  $\langle z \rangle = z_0$ , where  $z$  is the Cartesian coordinate in the direction perpendicular to the helium surface and

$$\langle z \rangle = \frac{\int d\mathbf{r} z \rho(\mathbf{r})}{\int d\mathbf{r} \rho(\mathbf{r})}, \quad (15)$$

we have added a constraint term to the energy  $E$  in Eq. (11). This constraint is equal to  $\lambda_c(\langle z \rangle - z_0)^2/2$ ,<sup>37-39</sup> where  $\lambda_c$  is an arbitrary constant large enough to ensure that upon minimization, the imposed value  $\langle z \rangle = z_0$  is obtained. This constrained minimization is needed to avoid the homogeneous liquid solution, which also has  $\mu = -7.145$  K. We have taken  $\lambda_c = 5 \times 10^5$  K Å<sup>-2</sup>, which ensures an optimal convergence rate. The desired  $z_0$  values are then obtained to within 0.1% accuracy.

The overall procedure is as follows: (i) Starting from a reasonable density guess, carry out a constrained minimization of the grand potential for a pristine PHeS with a  $z_0$  value well inside the calculation box. This has to be done only once, and it yields  $\Omega[\text{PHeS}]$  for the pristine helium surface. It can also be used to determine the surface tension of the helium surface, see next section. (ii) Repeat the procedure including the  $\text{A}^+$  ion at different  $z_{\text{A}^+}$  positions, and minimizing the grand potential with the same constraint  $\langle z \rangle = z_0$  as before. (iii) In the result of step (ii), determine the position  $z_{\text{surf}}$  of the sharp density surface at the box limits in the  $x$  or  $y$  direction (i.e., as far away from the ion as possible), and hence the distance  $d = z_{\text{A}^+} - z_{\text{surf}}$  of the ion from it.

## IV. RESULTS

The density profile of the pristine planar helium surface at equilibrium is plotted in Fig. 1 along the  $z$  direction, perpendicular to the surface. As mentioned above, the surface tension  $\gamma$  of the liquid can be evaluated from the equilibrium density. It is given by

$$\gamma = \frac{1}{\mathcal{S}} \int d\mathbf{r} [\mathcal{E}(\text{He}_{\text{PHeS}}) - \mu\rho(\text{He}_{\text{PHeS}})], \quad (16)$$

where  $\mathcal{S}$  is the area of the planar surface. The resulting value is  $\gamma = 0.278$  K Å<sup>-2</sup> with the functional used in this work.<sup>36</sup> It is in good agreement with the experimental value for  ${}^4\text{He}$ , 0.274 K Å<sup>-2</sup>.

Two-dimensional plots of the density for different distances  $d$  of the cation to the planar helium surface are displayed in Fig. 2 for  $\text{Na}^+$  and in Fig. 3 for  $\text{Ca}^+$ . The plane is perpendicular to the surface and contains the ion. Both figures reveal high-density structures around the ions. In addition, density lumps can be seen around the  $\text{Ca}^+$  ion due to spontaneous

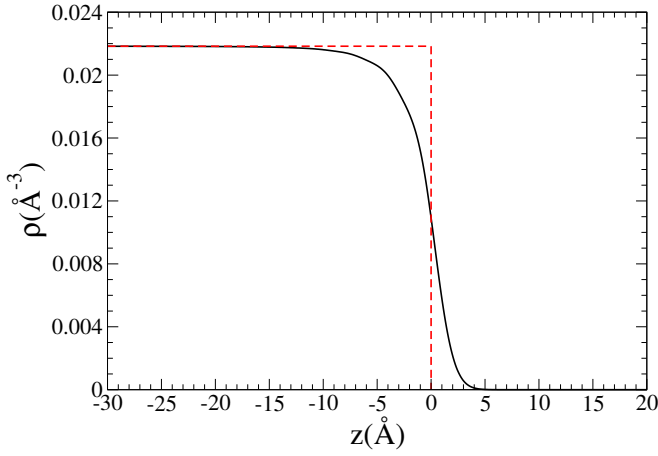


FIG. 1. Helium density profile in the direction  $z$  perpendicular to its planar surface. The origin of the  $z$ -axis is arbitrarily set at the location of the sharp density surface (red dashed line).

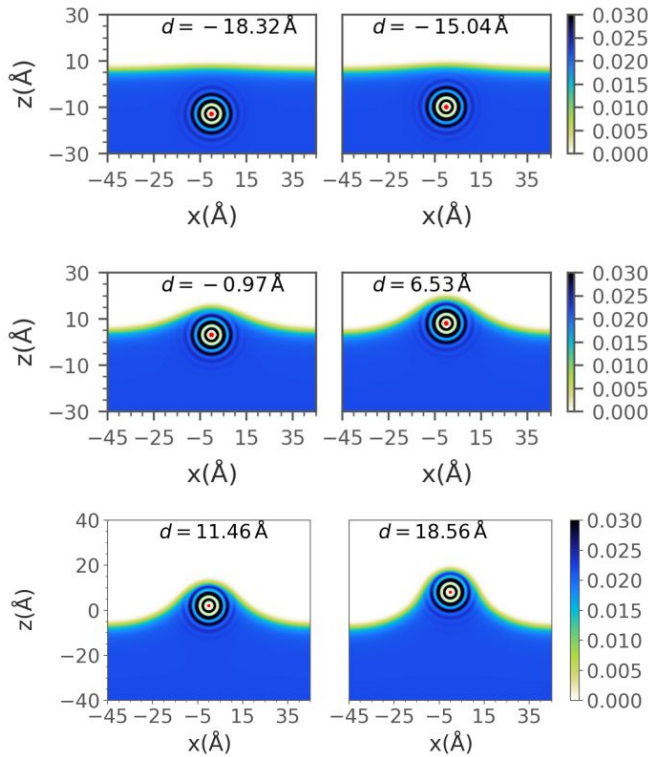


FIG. 2. Two-dimensional plots of the density corresponding to a planar He surface hosting a  $\text{Na}^+$  ion at a distance  $d$  from the sharp density surface. The color bar shows the density in units of  $\text{\AA}^{-3}$ . From left to right and from top to bottom:  $d = -18.32, -15.04, -0.97, 6.53, 11.46,$  and  $18.56 \text{ \AA}$ . Densities are shown in a plane perpendicular to the helium surface passing through the ion position.

symmetry breaking. This is not the case around the  $\text{Na}^+$  where spherical symmetry is conserved. Although the  $\text{Na}^+$ -He potential well is more attractive than the  $\text{Ca}^+$ -He one, it is narrower (see Fig. 4), which prevents the density lumps from developing.

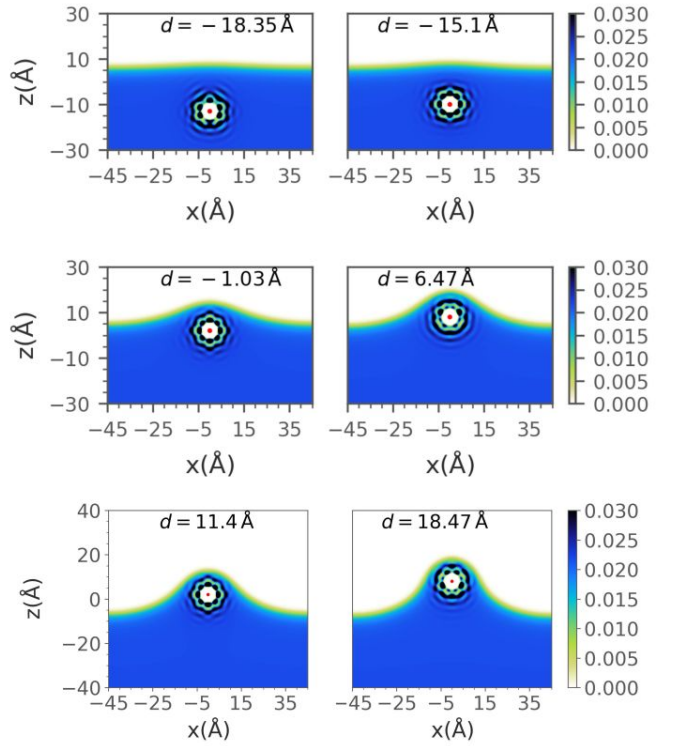


FIG. 3. Two-dimensional plots of the density corresponding to a planar He surface hosting a  $\text{Ca}^+$  ion at a distance  $d$  from the sharp density surface. The color bar shows the density in units of  $\text{\AA}^{-3}$ . From left to right and from top to bottom:  $d = -18.35, -15.10, -1.03, 6.47, 11.40,$  and  $18.47 \text{ \AA}$ . Densities are shown in a plane perpendicular to the helium surface passing through the ion position.

Another ingredient that plays an important role in the model is that of the microcluster, introduced in Eq. (1) and further defined following Eq. (7). As shown in a number of mass spectrometry experiments, ions produced by electron impact ionization of doped helium nanodroplets can be surrounded by many helium atoms.<sup>43</sup> The mass of the dopant as well as the ionization process and the settings of the ion source have a strong influence on the relative abundance of helium atoms around the dissociated ions. The situation described in the present simulations corresponds to the limit of very slow dissociation of the ions (“adiabatic” limit): the dissociating ions are solvated inside microclusters such as the ones starting to emerge out of the helium surface at the larger values of  $d$  in Figs 2-3. As long as these microclusters are still attached to the rest of the helium, even by a tiny density bridge, their chemical potential must be equal to that of bulk liquid, which determines the cluster size and grand potential  $\Omega_{micro}$ . The other extreme model would be that of infinitely fast dissociation of the ions (“infinite order sudden” approximation), where the ions would leave the droplet so fast that the surrounding helium could not follow and they would emerge as bare ions. Although a case of such fast dissociation has already been observed, it was in the very specific case of sudden ionization of alkali dimers sitting on a droplet surface,<sup>44–46</sup> where Coulomb repulsion was very strong and “solvation”

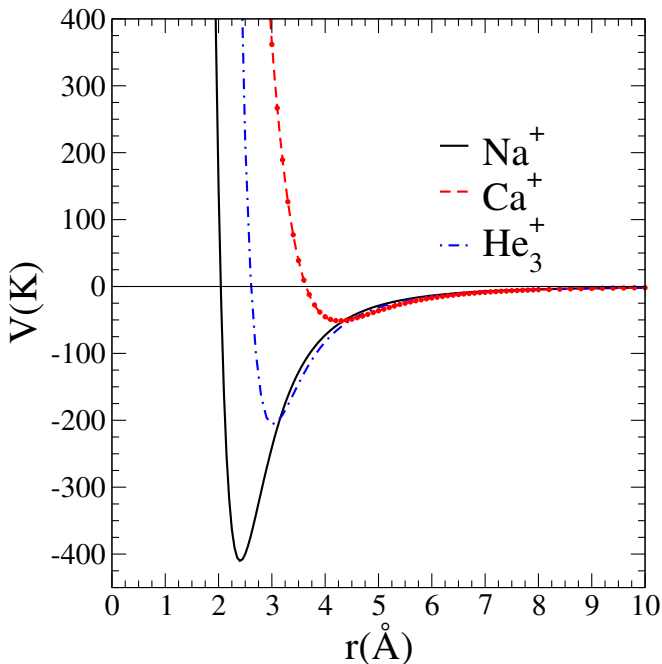


FIG. 4.  $\text{Na}^+$ -He pair potential,<sup>40</sup> spherically averaged  $\text{He}_3^+$ -He pair potential,<sup>5</sup> and  $\text{Ca}^+$ -He pair potential calculated in this work.

was very weak. Both these models, adiabatic and sudden, should be considered as opposite extremes of the same physical process, while the actual scenario as probed in experiments is likely in between. This should be considered when comparing our predictions with the experimental results, and could justify some quantitative discrepancies with our results, as will be discussed in the following.

In order to compute  $\Omega_{micro}$ , we have simulated the structure of the microcluster around the  $\text{Na}^+$  and the  $\text{Ca}^+$  ions separated from the PHeS, with the chemical potential set at the value of the bulk liquid and the number of helium atoms (i.e., the integral of the helium density) to be determined. Figure 5 shows the density profile of these microclusters. Notice the solid-like character of the first helium shell around  $\text{Na}^+$ , whereas the one around  $\text{Ca}^+$  looks more like that of a structured liquid. Both microclusters are fairly big: they contain a total of 105 helium atoms for  $\text{Na}^+$  and 93 for  $\text{Ca}^+$ . As can be seen in Fig. 5, they extend way beyond the first solvation shell, which contains 14 helium atoms for  $\text{Na}^+$  (values in the 9-16 atoms range are found using different approaches, see table II of Ref. 47), and 27 for  $\text{Ca}^+$  (close to the value of 25 found by Bartolomei et al.<sup>48</sup>). These large atom numbers are a likely consequence of the adiabatic approximation underlying the static constrained calculations of our approach.<sup>37-39</sup> In the real ejection dynamics, many of these atoms are stripped off the microcluster.<sup>49</sup>

We have determined the solvation energies  $S_d[\text{Na}^+@PHeS]$  and  $S_d[\text{Ca}^+@PHeS]$  for a number of values of the distance  $d$  of the ion to the sharp density planar surface from Eq. (6). The results are displayed in Fig. 6. In spite of the marked difference between the  $\text{Na}^+$ -He and  $\text{Ca}^+$ -He pair potentials, which can be seen in Fig. 4, the similarity between the solva-

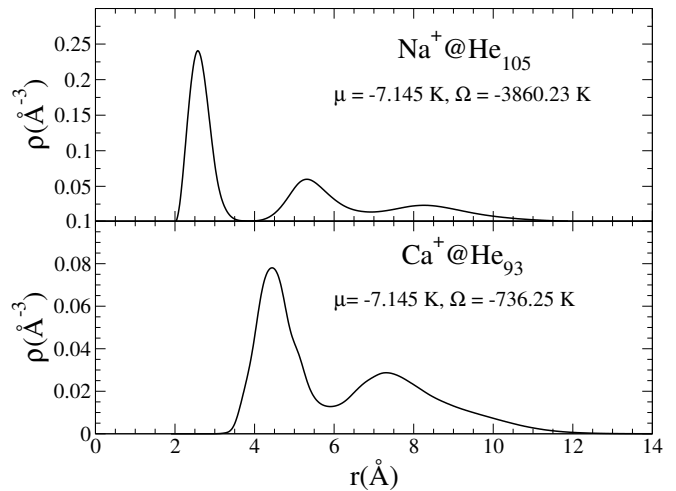


FIG. 5. Top panel: Density profile of the helium microcluster around a  $\text{Na}^+$  ion at chemical potential  $\mu = -7.145$  K. Bottom panel: Spherically averaged density profile of the helium microcluster around a  $\text{Ca}^+$  ion at chemical potential  $\mu = -7.145$  K. The integrated number of helium atoms and the value of the corresponding grand potential ( $\Omega$ ) are also given in the panels.

tion curves is remarkable. Considering Eq. (6), we can conclude that once  $\Omega_{micro}$  – the grand potential for the local structure around the ion – is subtracted from the grand potential  $\Omega_d[A^+@PHeS]$  of the overall system, the resulting solvation energy does not depend on the nature of the ion. This reflects the fact that the specificity of ion-helium interaction is responsible for the structure of the microcluster, and that beyond that structure, the ion-helium long distance interaction is species-independent, being that of a positive, elementary charge with helium (charge-induced dipole interaction). For this reason, from now on most of the results will only be discussed for the case of the  $\text{Na}^+$  ion.

We found it useful for the remainder of this work to fit the calculated values of  $S_d[\text{Na}^+@PHeS]$  and  $S_d[\text{Ca}^+@PHeS]$  to a simple analytic function. A very good fit has been obtained using the following expression

$$S_d[A^+@PHeS] = \frac{S_0}{\left[1 + \exp\left(\frac{d-d_0}{\sigma}\right)\right]^v} \quad (17)$$

with  $S_0 = -797.641$  K,  $\sigma = 9.262$  Å,  $d_0 = 16.627$  Å, and  $v = 1.234$  for  $\text{Na}^+$ ; and  $S_0 = -784.998$  K,  $\sigma = 9.431$  Å,  $d_0 = 19.486$  Å, and  $v = 1.533$  for  $\text{Ca}^+$ . As can be seen in Fig. 6, some departure of the fit from the actual He-DFT values only appears for large negative  $d$  values.

Notice that the solvation curves shown in Fig. 6 appear to flatten out for ion positions deep inside helium. On the contrary, mutual Coulomb repulsion increases strongly when ions get closer to the droplet center. As a consequence, if the charges are initially produced deep inside the droplet, they will move towards the surface until Coulomb repulsion is compensated by solvation energy.

Once  $S_d[\text{Na}^+@PHeS]$  has been calculated, it is straightforward to determine the radius of the smallest droplet hosting an

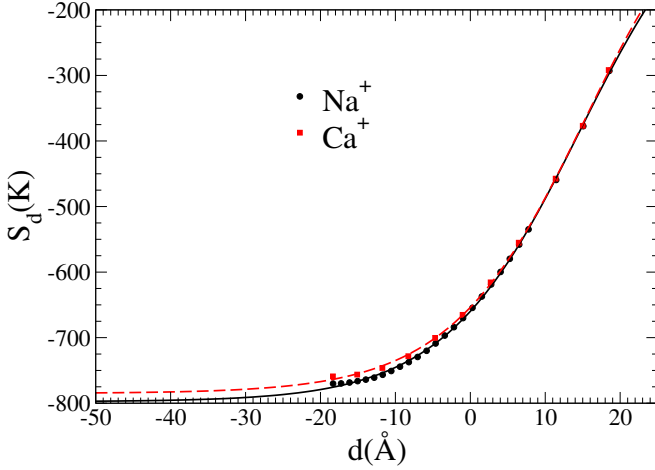


FIG. 6. He-DFT solvation energy of the ion as a function of its distance to the sharp density planar surface:  $S_d[Na^+@PHeS]$  (black dots) and  $S_d[Ca^+@PHeS]$  (red dots), and fit by Eq. (17):  $Na^+$  (solid, black line) and  $Ca^+$  (dashed, red line).

equilibrium distribution of  $n$  positive charges on its surface,  $R_0(n)$ , using Eq. (10). Figure 7 shows the results obtained for  $n = 2 - 10, 15$  and  $20$ . The behavior is the same for both cations. It reflects the fact that the minimum Coulomb energy of  $n$  charges on a sphere of radius  $R$  (Thomson's model) can be fitted by the empirical formula<sup>21</sup>

$$E_{Coul} = \frac{e^2}{4\pi\epsilon_0 R} \left[ \frac{n^2}{2} - 0.551n^{3/2} \right] \quad (18)$$

and therefore

$$R_0(n) \sim \frac{e^2}{4\pi\epsilon_0} \frac{1}{|S_d[A^+@PHeS]|} \left[ \frac{n}{2} - 0.551n^{1/2} \right]. \quad (19)$$

The minimum size for a droplet to contain  $n$  charges has been found to scale as  $n^{1/2}$  in experiments.<sup>3,4</sup> This is different from the dependence obtained here for the stability threshold radius  $R_0(n)$ . The resulting  $R_0(n)$  curve looks almost linear in Fig. 7, in part because of the small range of  $n$  values.

Other estimates have been proposed for the minimum size of charged liquid droplets that ensures stability against Coulomb repulsion. Livshits and Lozovik have addressed the crystallization and melting of a system of charges in a helium drop<sup>50</sup> within a LDM in which all charges are uniformly smeared over the spherical surface. Applying Rayleigh's criterion for the stability of a charged liquid droplet against surface oscillations,<sup>30</sup> they obtain for the critical radius [see Eq. (17) of Ref. 50]

$$R_c = \left[ \frac{e^2}{4\pi\epsilon_0} \frac{n^2}{16\pi\epsilon\gamma} \right]^{1/3}, \quad (20)$$

where  $\epsilon = 1.05$  is the dielectric constant of liquid  $^4\text{He}$ . For the sake of comparison with our results, we take  $\epsilon = 1$  and obtain  $R_c = 23n^{2/3}$  Å. Hence the scaling for the critical radius in this surface LDM plus Rayleigh model is then  $R_c \propto n^{2/3}$ , at variance with experiment.

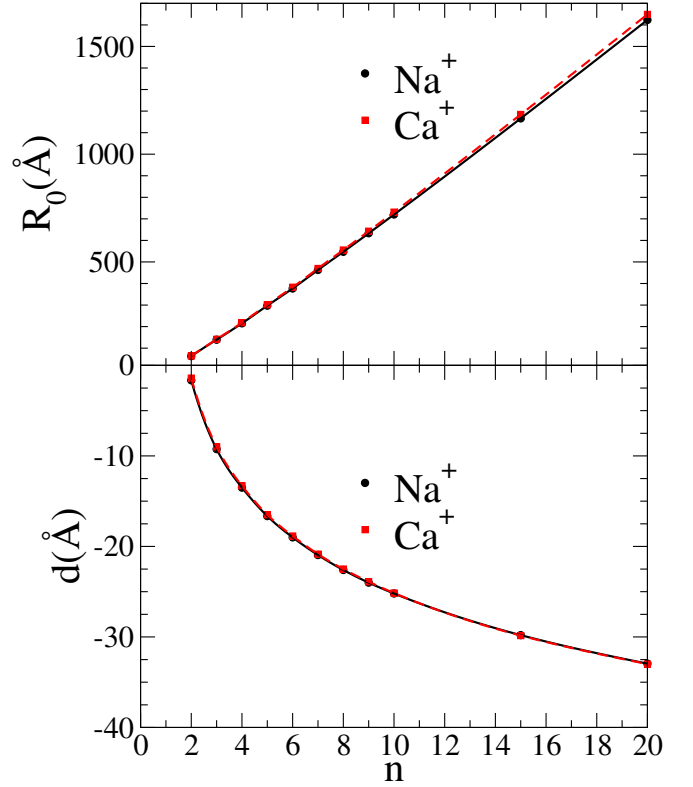


FIG. 7. Top panel: Limiting radius  $R_0$  (Å) for the stability of helium droplets hosting  $n$   $Na^+$  (black dots, black solid line) or  $Ca^+$  (red dots, dashed red line) ions for  $n = 2 - 10, 15$  and  $20$ . Bottom panel: distance  $d$  (Å) of the ions to the sharp density surface of the droplet.

We have checked an important assumption underlying the form of Eq. (9), namely that the equilibrium configurations of  $n$  charges on the droplet surface are solutions of Thomson's model. In particular, we wanted to check whether they shared the same common distance  $R + d$  from the droplet center.

In order to do that, we applied a Steepest-Descent (SD) algorithm to find the minimum energy configuration of  $n$  ions subject to solvation plus Coulomb forces in a droplet of radius  $R$ . In the iterative SD search algorithm, the positions  $\mathbf{r}_i$  ( $i = 1, n$ ) of the  $n$  ions were updated at each iteration as

$$\mathbf{r}_i^{k+1} = \mathbf{r}_i^k + \eta (\mathbf{F}_{solv,i}^k + \mathbf{F}_{coul,i}^k), \quad (21)$$

where  $\mathbf{F}_{coul,i}^k$  is the repulsive force acting on the  $i$ -th charge due to the other ions, and  $\mathbf{F}_{solv,i} = -(dS_d/dr)(\mathbf{r}/r)$  is the solvation force acting on the  $i$ -th charge due to the surrounding helium (attractive towards the droplet center), with  $S_d$  taken from Eq. (17). In addition,  $\eta$  is an arbitrary parameter to be adapted in order to speed up convergence: if it is too small, it takes very long to move downhill along a potential energy surface, and if it is too large one may have overshooting, i.e., the energy will increase from one step to the next. We have used  $\eta = 6 \times 10^{-5}$  Å<sup>2</sup>/K. Relation (21) was iterated until the forces cancelled out, i.e. an energy minimum was found, and hence the corresponding ion-droplet equilibrium distances. The initial ion positions were taken from the corresponding Thomson's structure with a small random displacement. The more

general displacements allowed by the SD dynamics lift the constraint of equal ion-center distance, even when the initial configuration is a solution of the Thomson model, allowing in principle for different radial displacements (“buckling”) or changes in the ions equilibrium positions on the droplet surface.

We found very small deviations with respect to the ideal Thomson’s structures, and very small energy gains. For instance, in the case of  $n = 20$   $\text{Na}^+$  ions on the surface of a helium nanodroplet of radius  $R = 250 \text{ \AA}$  (a value which –barely– guarantees Coulomb stability of the system), the average distance of the cations from the droplet center is  $\langle R + d \rangle = 235.4 \text{ \AA}$ , and the maximum excursion from the above value is  $\sim 0.8 \text{ \AA}$ . The gain in total energy with respect to the ideal solution is just 34 K over a total energy of  $\sim 10^4$  K. We have recalculated the  $R_0(n)$  curve using the SD scheme and found results virtually indistinguishable from those shown in Fig. (7).

Thomson’s model solutions with  $n$  charges are known to have a series of “magic” numbers, where the lowest-energy structures are particularly stable:<sup>25</sup>  $n = 12, 32, 72, 122, \dots$ . Most of these structures are icosahedral. We have verified that magic numbers are also present for the structures found in our SD minimization, by computing the second total energy (Coulomb + solvation) difference as a function of cluster charge

$$D_2[n] = E[n - 1] - 2E[n] + E[n + 1]. \quad (22)$$

Peaks in this quantity signal particularly stable structures. Two magic numbers,  $n = 12$  and 32, were found within the range explored here, in agreement with Thomson’s model.

Unexpectedly, during the SD optimization of ion positions, locally stable configurations were encountered for droplets with a radius smaller than the stability value  $R_0$ , hence for which ions should be ejected. These metastable configurations are a signal for the presence of energy barriers preventing ion ejection. In order to clarify this important issue, we examined the behavior of the energy  $U(r)$ ,  $r = R + d$ , using Eqs. (9) and (17).

Figure 8 shows  $U(r)$  for  $n = 2$  and different  $R$  values. One of the curves, corresponding to  $R = 63.17 \text{ \AA}$ , has a minimum with value  $U = 0$ , thus identifying  $R_0$ . Droplets with  $R > R_0$  (e.g.,  $R = 70 \text{ \AA}$  in the figure) are stable: they display a minimum with energy smaller than that of the reference system (i.e., a negative minimum). However,  $U(r)$  also displays a positive minimum for many  $R < R_0$  radii, separated by energy barriers from the dissociated configuration. These radii should correspond to *metastable* multicharged droplets, as their energy is higher than that of the reference system. These features are common to all the other  $n$  values investigated here.

For smaller and smaller  $R$  values, the barrier gradually decreases until disappearing: the charged droplet cannot be metastable anymore and ions are directly ejected off the droplet. For  $n = 2$  the critical radius at which the barrier disappears is  $R = 24.65 \text{ \AA}$ , as illustrated in Fig. 8. We call this radius the “explosion” radius  $R_{expl}$ . Its value for  $\text{Na}^+$  is plotted in Fig. 9 as  $n$  vs  $R_{expl}^2$  for the sake of comparison with experiment.

The barriers observed in Fig. 8 can be very high compared to thermal activation energy,  $E_{ther} = (3/2)k_B T$ , with  $k_B$  the Boltzmann constant. The highest barrier is for  $R = R_0$  ( $\sim 700$  K for two  $\text{Na}^+$  ions). In helium droplets  $T$  is very small, of the order of 0.4 K.<sup>1</sup> In view of this, we propose a sensible definition for the critical radius  $R_c(n)$  above which a droplet with  $n$  charges is stable at least up to the millisecond timescale of the experiments:<sup>3,4</sup>  $R_c$  is the radius of the droplet that displays an energy barrier equal to the thermal activation energy. Given the energy scale in Fig. 8,  $R_c \simeq R_{expl}$  in practice. For instance, for  $n = 20$  we have found that the barrier for  $R = 219.5 \text{ \AA}$  (which we have taken as  $R_{expl}$ ) is 0.06 K; for  $R = 219.65 \text{ \AA}$ , it is 0.67 K.

Also shown in Fig. 9 are the critical radii obtained by Livshits and Lozovik in the surface LDM plus Rayleigh instability approach,<sup>50</sup> Eq. (20) with  $\varepsilon = 1$ , as well as the experimental  $R_c$  values of Laimer *et al.* parameterized as<sup>3</sup>

$$n = a + \zeta R_c^2 \quad (23)$$

with  $a = -0.544$  and  $\zeta = 2.6 \times 10^{-2} \text{ nm}^{-2}$ . For the sake of comparison with the experimental results, we exceptionally give distances in nanometers in this figure and in the related discussion. As can be seen in Fig. 9,  $n$  depends linearly on  $R_{expl}^2$  in the He-DFT approach, in agreement with the experimental results, except for small  $n$  values for which curvature effects may be important. The results obtained in the surface LDM plus Rayleigh instability approach exhibit a different behavior ( $R_c^2 \propto n^{4/3}$ , see Eq. (20) and following text).

Figure 10 shows the distance of the  $\text{Na}^+$  cations to the surface of the droplet with  $R = R_{expl}$ . In all cases  $d > 0$ , meaning that the cations are above the droplet surface. For  $n \gtrsim 15$ , ions are  $\sim 15.5 \text{ \AA}$  away from the surface, giving the droplet a “virus-like” appearance, as shown for  $n = 20$  in the inset of the figure. Notice the nearly triangular arrangement of the ions on the droplet surface.

The experimentally observed relation between  $R_c$  and  $n$  for pristine helium droplets<sup>3</sup> is  $n \sim \zeta R_c^2$ , implying that the surface density of cations at which instability arises,

$$\mathcal{N} = n / (4\pi R_c^2) = \zeta / (4\pi), \quad (24)$$

is constant. This seems reasonable: any instability due to Coulomb repulsion must set in at the same critical charge surface density, irrespective of the droplet size. Using the experimental results of Ref. 3, one finds  $\mathcal{N}_{expt} = 2.07 \times 10^{-3} \text{ nm}^{-2}$ .

One can estimate the average distance  $\delta$  between neighboring ions on the droplet surface with critical radius  $R_c$ . Assuming that the  $n$  charges are arranged in a triangular lattice on the surface of the sphere (this is the expected structure for large values of  $n$ ), the surface area per particle is  $\Sigma = \sqrt{3}\delta^2/2$ ,  $\delta$  being the nearest-neighbor distance. The total area  $n\Sigma$  must be equal to  $4\pi R_c^2$ , i.e.  $n\sqrt{3}\delta^2/2 = 4\pi R_c^2$ , and therefore  $\delta = \sqrt{8\pi/(\sqrt{3}\zeta)}$ . Using the experimental value of  $\zeta$  one obtains  $\delta = 23.6 \text{ nm}$ . For  $n \gtrsim 10$  our results for  $R_{expl}$  also follow the law  $n = a' + \zeta' R_{expl}^2$  (see Fig. 9) with  $a' = 4.23$ ,  $\zeta' = 3.23 \times 10^{-2} \text{ nm}^{-2}$  and therefore  $\delta = 21.2 \text{ nm}$



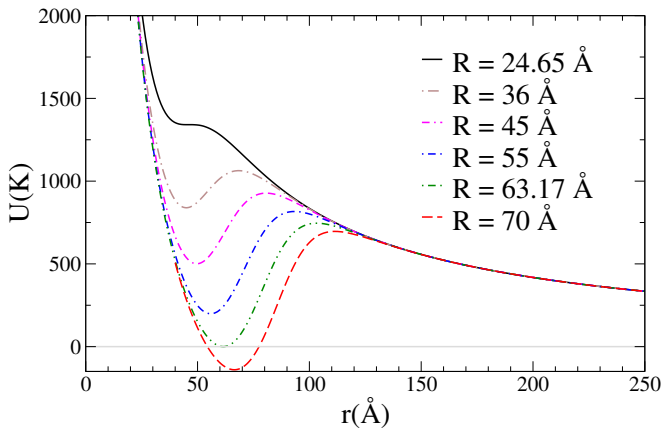


FIG. 8. Energy  $U(r)$  of a droplet hosting two  $\text{Na}^+$  ions as a function of the distance  $r$  of the ions to the center of the droplet. From top to bottom, the curves correspond to droplets with radius  $R=24.65$  ( $R_{expl}$ ), 36, 45, 55, 63.17 ( $R_0$ ), and 70 Å. The origin for energies is that of the reference (dissociated) system.

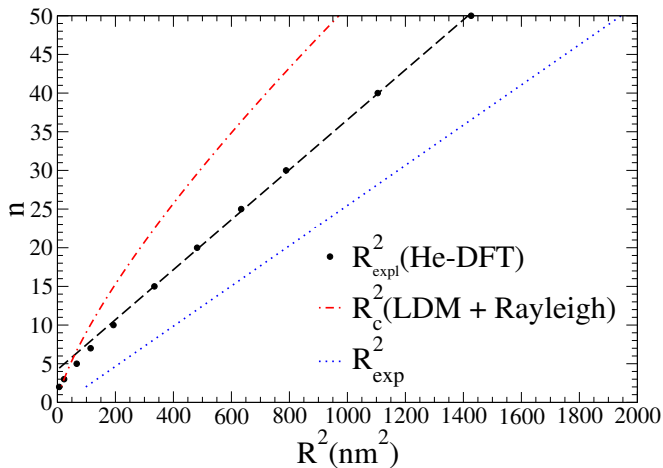


FIG. 9. Number of charges  $n$  vs  $R^2$  (in  $\text{nm}^2$ ). Black dots:  $R^2 = R_{expl}^2$  for  $\text{Na}^+$  in the He-DFT approach, with  $R_{expl}$  the minimum value below which multicharged droplets can no longer be even metastable (see text); dashed line: linear fit ( $n = a' + \zeta' R_{expl}^2$ ) to the results from  $n = 10$  to 50. Dotted line: experimental values<sup>3</sup>  $R^2 = R_c^2$ . Dash-dotted line:  $R^2 = R_c^2$  in the LDM plus Rayleigh instability approach.<sup>50</sup>

and  $\mathcal{N} = 2.57 \times 10^{-3} \text{ nm}^{-2}$ , similar to the experimental one for  $\text{He}_3^+$  ions.

## V. SUMMARY AND CONCLUDING REMARKS

We have designed a solvation plus Coulomb model for studying the stability of extrinsic multiply charged droplets, and applied it within the He-DFT approach. We believe that our approach is an improvement over those based on the liquid drop model plus Rayleigh's stability criterion, since it is built on a more accurate description of the solvation properties of

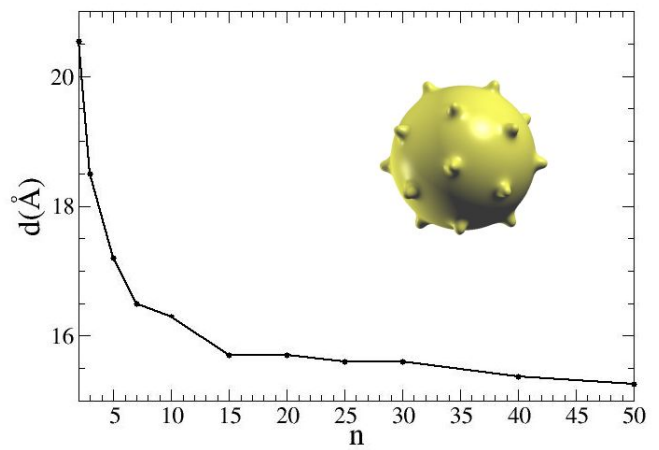


FIG. 10. Distance of the  $\text{Na}^+$  ion to the droplet surface as a function of the number of charges  $n$  for droplets of radius  $R_{expl}$ . The line has been drawn to guide the eye. The inset cartoon represents qualitatively the actual shape of a droplet with  $n = 20$  and a radius close to  $R = R_{expl}$ . The density is approximately obtained by superimposing a finite-width He density profile mimicking the one in Fig. 1 with gaussian profiles centered around each cation.

positive ions in helium. In particular, it explicitly takes into account the ion-snowball microclusters which are eventually ejected after Coulomb explosion as found in the experiments.

In addition to the stability study, we have disclosed the existence of energy barriers in the dissociation process of the ion microclusters from the helium droplet. These barriers explain why multiple ions-droplet systems can be observed for droplet sizes smaller than predicted for their stability: they are metastable, at least during the millisecond time range of the experiments.

We have defined the critical radius for the (meta)stability of multicharged droplets as that for which the energy barrier equals the thermal activation energy. This critical radius can be identified in practice with the radius  $R_{expl}$  for which the charged droplet would undergo Coulomb explosion.

We have found that close to the critical radius, charges are localized just above the helium surface, resulting in a virus-like appearance of the critical multicharged helium droplet. For radii increasingly larger than the critical one, charges submerge but still remain close to the droplet surface.

It is interesting to note that the energy barriers result from the interplay between ion solvation and Coulomb energies. This is at variance with nuclear fission barriers, where the interplay is between surface and Coulomb energies.<sup>26</sup> Yet, a proper description of the droplet surface, such as the one provided by modern density functionals,<sup>32,36</sup> was essential here to take surface tension correctly into account.

Considering helium droplets doped with  $\text{Na}^+$  or  $\text{Ca}^+$  ions as study cases, we conclude that the results are rather species independent. Hence it is very tempting to compare our results with those obtained for pristine drops,<sup>3</sup> even though the mechanisms for producing extrinsic and intrinsic multicharged helium droplets are different. The results obtained here reproduce the linear dependence of the number of hosted ions with

the square of the critical radius. However, the agreement is qualitative, our values for  $R_{expl}$  being systematically smaller than the experimental critical radius for intrinsic multicharged helium droplets.<sup>3</sup> The agreement is still better than the one found with the LDM plus Rayleigh stability criterion of a charged liquid droplet,<sup>50</sup> which in addition does not reproduce the linear behaviour of  $n$  vs  $R^2$ .

It is worth stressing that we have carried out static calculations to determine the energy barriers and critical radii. In the real world, the process is dynamic: for intrinsic multiply charged helium droplets,  $\text{He}_3^+$  ions are produced by electron impact near the surface facing the electron source<sup>3,6</sup> and readjust under the Coulomb repulsion to locations similar to Thomson’s model configurations in order to minimize the total energy. Some of these charges may have enough kinetic energy to leave the droplet. Consequently, the critical radius is expected to be larger than in our predictions based on static models where charges are supposed to be evenly distributed on the droplet surface. However, considering an Atkins’ snowball of 200 amu mass<sup>5</sup> moving at a maximum velocity of the order of Landau’s velocity, say 50 m/s, its kinetic energy is only about 30 K, so one should not expect a large effect on the critical radius. For instance, in the case of  $n = 2$  a barrier of 30 K appears in the  $R = 27.1 \text{ \AA}$  droplet, only  $2.5 \text{ \AA}$  larger than  $R_{expl}$ .

Even within our static approach, we can get a flavor of what the effect of the ionization dynamics could be. Taking advantage of the fact that steepest-descent minimization usually yields the closest local minimum, we have obtained metastable configurations with an energy higher than that of the absolute minimum (the solution of Thomson’s model) by starting the SD procedure from a distribution of ions inside the bulk of a droplet. For instance, if we start with  $n = 20$  ions distributed within a droplet of radius  $R = 350 \text{ \AA}$  (large enough to guarantee the stability of the droplet-ions system), we end up with a surface distribution of the positive ions but with an energy higher by  $\sim 730 \text{ K}$  than that of the solution of Thomson’ model, which is  $5.879 \times 10^4 \text{ K}$ . This metastable configuration is buckled, i.e., all the ions do not reside at the same distance from the droplet center: the maximum difference is  $\sim 4 \text{ \AA}$ . The calculated value for the critical radius is then larger than the one obtained from the ideal Thomson configuration,  $R_{expl} = 254 \text{ \AA}$  instead of  $221 \text{ \AA}$ , but it is still smaller than the experimental  $R_c$  value of  $\sim 281 \text{ \AA}$ .<sup>3</sup> Interestingly, for a droplet with a radius slightly smaller than  $254 \text{ \AA}$ , Coulomb explosion occurred differently from the symmetric dynamics of the “ideal” structure where all cations move radially away from the droplet. For this metastable configuration, only one cation was expelled, and the remaining 19 ones readjusted their positions and remained on the surface of the droplet.

Another possible source of discrepancies between our calculations and experiments is our substitution of the droplet geometry by a planar surface in order to compute the solvation energy. This would mainly affect the predicted  $R_{expl}$  values for small  $n$  charged drops, where curvature effects are more important.

We acknowledge that it might not be easy to carry out an experiment on extrinsic multiply charged helium droplets ob-

	$\text{Ca}^+-\text{He}$	$\text{He}_3^+-\text{He}$
$g_1$	$9.71136 \times 10^6$	$1.17674 \times 10^7$
$g_2$	$-1.68041 \times 10^7$	$-1.77677 \times 10^7$
$g_3$	$1.12045 \times 10^7$	$1.15284 \times 10^7$
$g_4$	$-3.20735 \times 10^6$	$-3.65381 \times 10^6$
$g_5$	$8.79979 \times 10^4$	$2.66532 \times 10^5$
$g_6$	$1.71418 \times 10^5$	$1.41737 \times 10^5$
$g_7$	$-3.10192 \times 10^4$	$-2.19406 \times 10^4$
$g_8$	-46.583	-555.796
$g_9$	261.538	-138.371
$\alpha$	3.443	6.109
$\beta$	-2.858	-8.837
$C_4$	$1.54022 \times 10^4$	$1.81590 \times 10^4$
$C_6$	$3.37909 \times 10^5$	$1.74591 \times 10^4$
$C_8$	$-1.73043 \times 10^6$	$4.57316 \times 10^5$

TABLE I. Parameters of the  $\text{Ca}^+-\text{He}$  and  $\text{He}_3^+-\text{He}$  pair potentials, Eqs. (A2) and (A3).

tained from droplets doped with alkali or the heavier alkaline earth atoms, due to their tendency to form clusters and sink inside the droplet. This might happen before the dopant atoms are ionized, hampering the formation of the initial multi-ion configuration object of this study. Yet, we hope that our results on extrinsic multiply charge drops will motivate further experiments for determining if there is a quantitative difference between them and those on intrinsic multiply charged drops and if yes, what the origin could be.

## Appendix A: Interaction pair potentials

The potential energy surface (PES) of the  $\text{Ca}^+-\text{He}$  system have been determined at the CCSD(T) level of theory, adopting high quality basis sets and a fine grid of internuclear distances. When performing first principles computations, we explicitly considered all 21 electrons (19 belonging to  $\text{Ca}^+$  and 2 to He) to evaluate the electron correlation contribution to the interaction energy. All data have been corrected for basis set superposition error using the well-known counterpoise procedure proposed by Boys and Bernardi.<sup>51</sup> As for the basis set, we adopted the all-electrons Def2-QZVPPD<sup>52</sup> for calcium, and the aug-cc-pVQZ<sup>53</sup> for helium. To approach the limit of basis set completeness, they have been supplemented with a  $3s3p2d$  basis of bond functions<sup>54</sup> placed at midway between the  $\text{Ca}^+$  and the He nuclei. To test the reliability of the basis set choice, we performed two limited series of test computations. The electrons of helium have been described with the aug-cc-pV5Z<sup>53</sup> set as well as with the aug-cc-pV6Z<sup>55</sup> one. In both cases the relevant features of the PES undergo negligible variations. The  $\text{Ca}^+-\text{He}$  separation of the minimum interaction energy varies by less than  $0.01 \text{ \AA}$ , and the same holds true for the turning point, i.e. the distance where the PES reverts from attractive to repulsive. Accordingly, the depth of the attractive well increases by about 0.5%. Overall, data obtained with the three different basis sets for He are almost identical, whatever the internuclear distance considered. A

test on the theoretical method has been conducted as well. Following a procedure well grounded in the case of weakly bound complexes,<sup>56,57</sup> we evaluated the electron correlation contribution of the three outermost electrons ( $4s^1$  belonging to  $\text{Ca}^+$ ,  $1s^2$  to He) at the Full-Configuration-Interaction (FCI) level of theory. To get a reliable interaction potential, the FCI results have been summed up to the contribution of the 18 inner electrons, which has been evaluated with the CCSD(T) approach. Also in this case no relevant change in the PES has been recorded. We are therefore confident that our computational scheme is capable of describing the  $\text{Ca}^+$ -He complex with a high degree of accuracy. To determine the entire PES, we defined a spatial grid consisting in 100 internuclear separations, such as to sample finely (i.e. with 0.10 Å steps) the repulsive wall and the attractive well, while enlarging the grid in the long-range tail.

The overall properties of the PES can be summarized as follows: (i) the depth of the attractive well amounts to 35.92  $\text{cm}^{-1}$ ; (ii) the minimum interaction energy is located at the  $\text{Ca}^+$ -He distance of 4.27 Å; (iii) the PES reverts from being attractive to repulsive at 3.64 Å and (iv) the repulsive wall reaches  $10^3 \text{ cm}^{-1}$  at 2.43 Å. These data agree very well with a recent study on this same complex,<sup>48</sup> and they are consistent with available results obtained at a slightly lower level of theory.<sup>58,59</sup>

The *ab initio*  $\text{Ca}^+$ -He pair potential has been fit to an analytical expression similar to that of Buchachenko et al.<sup>60</sup>

$$V(r) = V_{SR}(r) + V_{LR}(r), \quad (\text{A1})$$

where

$$V_{SR}(r) = \left[ \sum_{i=1}^9 g_i r^{(i-1)} \right] e^{(-\alpha r - \beta)} \quad (\text{A2})$$

represents a short-range repulsive interaction, and  $V_{LR}$  corresponds to a long-range attractive interaction. For ions,

$$V_{LR}(r) = \frac{C_4}{r^4} + \frac{C_6}{r^6} + \frac{C_8}{r^8} \quad (\text{A3})$$

The parameters were determined using a nonlinear least-squares algorithm. The value of the parameters is given in Table I. For the sake of completeness, we also give the parameters of the spherically averaged  $\text{He}_3^+$ -He pair potential of Ref. 5, the raw data of which have been obtained by digitizing the curve in Fig. 4 of that reference. Units of the parameters are such that when  $r$  is given in Å,  $V(r)$  is obtained in K. The *ab initio* points and fit are shown in Fig. 4. The overall quality of the fits is very good.

## ACKNOWLEDGMENTS

We thank Paul Scheier and Marcel Mudrich for useful discussions. A computer grant from CALMIP high performance computer center (grant P1039) is gratefully acknowledged. This work has been performed under Grant No. PID2020-114626GB-I00 from the

MICIN/AEI/10.13039/501100011033 and benefited from COST Action CA21101 “Confined molecular systems: from a new generation of materials to the stars” (COSY) supported by COST (European Cooperation in Science and Technology).

## AUTHOR DECLARATIONS

### Conflict of Interest

The authors have no conflicts to disclose.

## DATA AVAILABILITY

The data that support the findings of this study are available from the corresponding author upon reasonable request.

- <sup>1</sup>J. P. Toennies and A. F. Vilesov, *Angew. Chem. Phys.* **43**, 2622 (2004).
- <sup>2</sup>M. Fárník, U. Henne, B. Samelin, and J. P. Toennies, *Z. Phys. D* **40**, 93 (1997).
- <sup>3</sup>F. Laimer, L. Kranabetter, L. Tiefenthaler, S. Albertini, F. Zappa, A. M. Ellis, M. Gatchell, and P. Scheier, *Phys. Rev. Lett.* **123**, 165301 (2019).
- <sup>4</sup>A. J. Feinberg, F. Laimer, R. M. P. Tanyag, B. Senfftleben, Y. Ovcharenko, S. Dold, M. Gatchell, S. M. O. O’Connell-Lopez, S. Erukala, C. A. Saladrigas, B. W. Toulson, A. Hoffmann, B. Kamerin, R. Boll, A. De Fanis, P. Grychtol, T. Mazza, J. Montano, K. Setoodehnia, D. Lomidze, R. Hartmann, Ph. Schmidt, A. Ulmer, A. Colombo, M. Meyer, T. Möller, D. Rupp, O. Gessner, P. Scheier, and A. F. Vilesov, *Phys. Rev. Research* **4**, L022063 (2022).
- <sup>5</sup>D. Mateo and J. Eloranta, *J. Phys. Chem. A* **118**, 6407 (2014).
- <sup>6</sup>A. M. Ellis and S. Yang, *Phys. Rev. A* **76**, 032714 (2007).
- <sup>7</sup>A. Mauracher, O. Echt, A. M. Ellis, S. Yang, D. K. Bohme, J. Postler, A. Kaiser, S. Denifl, and P. Scheier, *Phys. Rep.* **751**, 1 (2018).
- <sup>8</sup>J. Tiggesbäumker and F. Stienkemeier, *Phys. Chem. Chem. Phys.* **9**, 4748 (2007).
- <sup>9</sup>J. Eloranta and V. A. Apkarian, *J. Chem. Phys.* **117**, 10139 (2002).
- <sup>10</sup>V. Grau, M. Barranco, R. Mayol, and M. Pi, *Phys. Rev. B* **73**, 064502 (2006).
- <sup>11</sup>H. J. Maris, *J. Phys. Soc. Jpn.* **77**, 111008 (2008).
- <sup>12</sup>F. Ancilotto, E. Cheng, M. W. Cole, and F. Toigo, *Z. Phys. B* **98**, 823 (1995).
- <sup>13</sup>F. Stienkemeier, J. Higgins, C. Callegari, S. I. Kanorsky, W. E. Ernst, and G. Scoles, *Z. Phys. D* **38**, 253 (1996).
- <sup>14</sup>O. Bünermann, G. Droppelmann, A. Hernando, R. Mayol, and F. Stienkemeier, *J. Phys. Chem. A* **111**, 12684 (2007).
- <sup>15</sup>A. Hernando, R. Mayol, M. Pi, M. Barranco, F. Ancilotto, O. Bünermann, and F. Stienkemeier, *J. Phys. Chem. A* **111**, 7303 (2007).
- <sup>16</sup>S. Vongehr, A. A. Scheidemann, C. Wittig, and V. V. Kresin, *Chem. Phys. Lett.* **353**, 89 (2002).
- <sup>17</sup>P. Schulz, P. Claas, D. Schumacher, and F. Stienkemeier, *Phys. Rev. Lett.* **92**, 013401 (2004).
- <sup>18</sup>C. Stark and V. V. Kresin, *Phys. Rev. B* **81**, 085401 (2010).
- <sup>19</sup>L. Tiefenthaler, J. Ameixa, P. Martini, S. Albertini, L. Ballauf, M. Zankl, M. Goulart, F. Laimer, K. von Haeften, F. Zappa, and P. Scheier, *Rev. Sci. Instrum.* **91**, 033315 (2020).
- <sup>20</sup>A. Leal, D. Mateo, A. Hernando, M. Pi, M. Barranco, A. Ponti, F. Cargnoni, and M. Drabbels, *Phys. Rev. B* **90**, 224518 (2014).
- <sup>21</sup>T. Erber and G. M. Hockney, *J. Phys. A: Math. Gen.* **24**, L1369 (1991).
- <sup>22</sup>J. Tempere, I. F. Silvera, and J. T. Devreese, *Surf. Sci. Repts.* **62**, 159 (2007).
- <sup>23</sup>W. Guo, D. Jin, and H. J. Maris, *Phys. Rev. B* **78**, 014511 (2008).
- <sup>24</sup>N. Yadav, P. Sen, and A. Ghosh, *Sci. Adv.* **7**, eabi7128 (2021).
- <sup>25</sup>J. R. Morris, D. M. Deaven, and K. M. Ho, *Phys. Rev. B* **53**, R1740 (1996).

- <sup>26</sup>A. Bohr and B. R. Mottelson, *Nuclear Structure*, vol. II, appendix 6A p. 66. World Sci., Singapore (1998).
- <sup>27</sup>O. Echt, D. Kreisler, E. Recknagel, J. J. Saenz, R. Casero, and J. M. Soler, *Phys. Rev. A* **38**, 3236 (1988).
- <sup>28</sup>F. Garcias, A. Mañanes, J. M. Lopez, J. A. Alonso, and M. Barranco, *Phys. Rev. B* **51**, 1897 (1995).
- <sup>29</sup>U. Näher, S. Bjørnholm, S. Frauendorf, F. Garcias, and C. Guet, *Phys. Rep.* **285**, 245 (1997).
- <sup>30</sup>Lord Rayleigh, *Philos. Mag.* **14**, 184 (1882).
- <sup>31</sup>I. Mähr, F. Zappa, S. Denifl, D. Kubala, O. Echt, T. D. Märk, and P. Scheier, *Phys. Rev. Lett.* **98**, 023401 (2007).
- <sup>32</sup>F. Dalfovo, A. Latri, L. Pricauptenko, S. Stringari, and J. Treiner, *Phys. Rev. B* **52**, 1193 (1995).
- <sup>33</sup>M. Barranco, R. Guardiola, S. Hernández, R. Mayol, J. Navarro, and M. Pi, *J. Low Temp. Phys.* **142**, 1 (2006).
- <sup>34</sup>F. Ancilotto, M. Barranco, F. Coppens, J. Eloranta, N. Halberstadt, A. Hernandez, D. Mateo, and M. Pi, *Int. Rev. Phys. Chem.* **36**, 621 (2017).
- <sup>35</sup>M. Barranco, F. Coppens, N. Halberstadt, A. Hernandez, A. Leal, D. Mateo, R. Mayol, and M. Pi, *Zero temperature DFT and TDDFT for <sup>4</sup>He: A short guide for practitioners*. <https://github.com/bcctl1s2016/DFT-Guide/blob/master/dft-guide.pdf>
- <sup>36</sup>F. Ancilotto, M. Barranco, F. Caupin, R. Mayol, and M. Pi, *Phys. Rev. B* **72**, 214522 (2005).
- <sup>37</sup>A. Hernandez, M. Barranco, R. Mayol, M. Pi, and F. Ancilotto, *Phys. Rev. B* **78**, 184515 (2008).
- <sup>38</sup>A. Leal, X. Zhang, M. Barranco, F. Cargnoni, A. Hernandez, D. Mateo, M. Mella, M. Drabbels, and M. Pi, *J. Chem. Phys.* **144**, 094302 (2016).
- <sup>39</sup>F. Coppens, A. Leal, M. Barranco, N. Halberstadt, and M. Pi, *J. Low Temp. Phys.* **187**, 439 (2017).
- <sup>40</sup>A. D. Koutselos, E. A. Mason, and L. A. Viehland, *J. Chem. Phys.* **93**, 7125 (1990).
- <sup>41</sup>M. Pi, F. Ancilotto, F. Coppens, N. Halberstadt, A. Hernandez, A. Leal, D. Mateo, R. Mayol, and M. Barranco, *4He-DFT BCN-TLS: A Computer Package for Simulating Structural Properties and Dynamics of Doped Liquid Helium-4 Systems*. <https://github.com/bcctl1s2016/>
- <sup>42</sup>M. Frigo and S.G. Johnson, *Proc. IEEE* **93**, 216 (2005).
- <sup>43</sup>T. González-Lezana, O. Echt, M. Gatchell, M. Bartolomei, J. Campos-Martínez, and P. Scheier, *Int. Rev. Phys. Chem.* **39**, 465 (2020).
- <sup>44</sup>H. H. Kristensen, L. Kranabetter, C. A. Schouder, C. Stapper, J. Arlt, M. Mudrich, and H. Stapelfeldt, *Phys. Rev. Lett.* **128**, 093201 (2022).
- <sup>45</sup>H. H. Kristensen, L. Kranabetter, C. A. Schouder, J. Arlt, F. Jensen, and H. Stapelfeldt, *Phys. Rev. A* **107**, 023104 (2023).
- <sup>46</sup>E. García-Alfonso et al., unpublished.
- <sup>47</sup>E. García-Alfonso, M. Barranco, N. Halberstadt, and M. Pi, *J. Chem. Phys.* **160**, 164308 (2024).
- <sup>48</sup>M. Bartolomei, P. Martini, R. Pérez de Tudela, T. González-Lezana, M. I. Hernández, J. Campos-Martínez, J. Hernández-Rojas, J. Bretón, and P. Scheier, *Molecules* **26**, 3642 (2021).
- <sup>49</sup>S. H. Albrechtsen, C. A. Schouder, A. Viñas-Muñoz, J. K. Christensen, C. E. Petersen, M. Pi, M. Barranco, and H. Stapelfeldt, *Nature* **623**, 319 (2023).
- <sup>50</sup>A. M. Livshits and Yu. E. Lozovik, *J. Exp. Theor. Phys.* **105**, 571 (2007).
- <sup>51</sup>S. F. Boys and F. Bernardi, *Mol. Phys.* **19**, 553 (1970).
- <sup>52</sup>D. Rappoport and F. Furche, *J. Chem. Phys.* **133**, 134105 (2010)
- <sup>53</sup>D. E. Woon and T. H. Dunning Jr., *J. Chem. Phys.* **100**, 2975 (1994).
- <sup>54</sup>F.-M. Tao and Y.-K. Pan, *J. Chem. Phys.* **97**, 4989 (1992).
- <sup>55</sup>T. Van Mourik, A. K. Wilson, and T. H. Dunning Jr., *Mol. Phys.* **96**, 529 (1999).
- <sup>56</sup>R. J. Hinde, *J. Phys. B* **36**, 3119 (2003).
- <sup>57</sup>J. M. L. Martin and P. R. Taylor, *Chem. Phys. Lett.* **225**, 473 (1994).
- <sup>58</sup>E. Czuchaj, F. Reberntrost, H. Stoll, and H. Preuss, *Chem. Phys.* **207**, 51 (1996).
- <sup>59</sup>S. L. Fiedler, D. Mateo, T. Aleksanyan, and J. Eloranta, *Phys. Rev. B* **86**, 144522 (2012).
- <sup>60</sup>A. A. Buchachenko, T. V. Tscherbul, J. Kłos, M. M. Szczeniński, G. Chałasiński, R. Webb, and L. A. Viehland, *J. Chem. Phys.* **122**, 194311 (2005).